Hindawi
Advances in Civil Engineering
Volume 2023, Article ID 7305238, 12 pages
https://doi.org/10.1155/2023/7305238

Research Article

The Effect of Different Fibers on Granite Residual Soil Reinforced with Alkaline Solution

Bingxiang Yuan,[1] **Jianhong Liang**,[1] **Jingkang Liang**,[1] **Weijie Chen**,[1] **Baifa Zhang**,[1] **Wei Chen**,[2] **and Tianying Chen**[1]

[1]*School of Civil and Transportation Engineering, Guangdong University of Technology, Guangzhou 510006, China*
[2]*School of Civil Engineering, Southeast University, Nanjing, China*

Correspondence should be addressed to Baifa Zhang; zhangbaifa@gdut.edu.cn

Received 7 September 2022; Revised 8 February 2023; Accepted 22 March 2023; Published 6 April 2023

Academic Editor: Danqing Song

This study explores the reinforcement effect of different fibers in an alkaline solution on the mechanical properties of granite residual soil using the single variable method. The macroscopic mechanical properties of the reinforced samples were studied using the unconfined lateral compressive strength test and the drop-weight load test, while the microscopic properties were characterized using techniques such as SME and XRD. The results indicated that the greatest reinforcing effect was attained when the ratio of SiO_2/Na_2O in the alkaline solution was 0.5 mol with the compressive strength of 4402.85 kPa. At the time, the reinforcing effect of glass fiber in an alkaline solution on granite residual soil was superior to that of basalt fiber. The inclusion of glass fibers and an alkaline solution of 0.5 mol SiO_2/Na_2O into the granite residual soil exhibited the best capacity for reinforcing, with the maximum impact load and compression reaching 120 kN and 12.1 mm, respectively. The findings of SME analysis revealed that GRS included a significant amount of kaolinite, which, when decomposed in an alkaline solution, generated a gel substance that bound the fibers and soil together and filled the pores between them, thereby enhancing the sample's compactness. XRD results demonstrated the formation of gel and a small amount of geopolymer in the soil under the alkaline solution of 0.5 mol SiO_2/Na_2O, which tighten the binding between soil particles and fibers and increase the overall strength.

1. Introduction

As China's economy is booming, the number of people living in urban areas increases, necessitating a rise in public transportation usage. Large public construction projects produce substantial amounts of construction waste. Up to two million tons of waste soil were generated in 2019 [1]. However, construction waste soil disposal has become a cause for concern. In general, only a small proportion of excavated waste soil can be utilized for low-level highways or infrastructure pit backfill; the bulk must be transferred to a landfill. This will inevitably result in a series of consequences. The release of soil particles during transportation endangers the local community's health by contaminating the road and the surrounding air environment. In addition, a large number of waste soil landfills consume a great deal of space, resulting in a tremendous waste of land resources. Therefore, the sustainable utilization of construction waste soil is a contemporary and environmentally-friendly topic [2]. Investigating a suitable approach to utilize the soil has major practical engineering significance because it can both alleviate the issue of random waste soil disposal and minimize energy usage [3].

The recycling of waste soils is generally popular among academics [4–6]. Several of these studies were instructive and prospective. The compressive strength of the reinforced kaolin clay samples significantly increased when industrial wastes such as steel slag and slag were employed as raw materials to strengthen the residual soil, together with activated magnesium oxide and calcium oxide [7]. Using scientific processes, cement blocks and waste granite cutting slag were regenerated with comparable strength to cement

blocks [8]. Construction waste has been converted into geogrids with certain tensile strength using a special technique [9]. The addition of kaolinite-containing waste soil to concrete increased its strength while decreasing the amount of cement required [10]. All of them indicate that the sustainable utilization of construction waste soil has attracted considerable attention.

Due to the unique geographical location and climate of South China, the majority of the construction waste soils in this region, including Guangdong and Fujian, are granite residual soils (GRS), which feature a very high bearing capacity under dry conditions but tend to soften and the bearing capacity decreases abruptly when exposed to water [11–13]. The region of South China is characterized by a hot and humid climate; hence, GRS is frequently regarded as a waste soil since its bearing capacity falls below the requirement upon contact with water due to its high porosity and hydrophilic kaolinite content [14]. Because of this, GRS is prone to soften in water, resulting in a loss of bearing capacity [15], making it difficult to preserve its original form [16–18]. In order to reuse GRS in a sustainable way, researches on mitigating the water disintegration property of GRS have been undertaken, including the use of polymer SH, which attaches a layer of hydrophobic groups to the surface of kaolinite to maintain its strength when exposed to water [19–25]. Some domestic studies have shown that transparent soil will also have similar characteristics to GRS under the action of alkali solution and cement [26–30]. At the same time, there is similar research abroad [31–34]. Others have used alkaline solutions to consume kaolinite in GRS in order to essentially remove its hydrophilicity and ensure its strength [35, 36]. Alternatively, numerous studies have resolved the issue by reinforcing GRS with fly ash or cement [37] to increase its compressive strength. Although methods such as adding cement or fly ash to GRS can boost its strength, they are rarely environmentally friendly enough, and the process generates significant carbon emissions [38, 39]. Therefore, it is essential to consider more sustainable reinforcing solutions.

Environmentally friendly and nonpolluting, alkaline solution is an inorganic solution that, at the right ratio, can be used to consume kaolinite in GRS and generate a geopolymer or gel substances. Since kaolinite has been consumed, this substance not only improves the soil to some degree but also solves the problem of GRS disintegrating rapidly in water [14, 40, 41]. Alkaline treatment of GRS has a number of advantages, but the treated GRS is exceptionally brittle, which could lead to a brittle effect comparable to that of cement reinforcement [42–44]. For this reason, the use of this material for large-scale applications is discouraged. [45–49]. Fiber has been studied as a potential solution for the brittleness of treated GRS. The addition of fibers from waste tire, sisal, cactus pulp, bamboo, and polypropylene has been demonstrated to decrease brittleness and increase the stress between soil particles and bearing capacity [50–55].

From the aforementioned literature, it is clear that although these researchers have made contributions to the field of reinforcing soils with fibers or other agents, there is a dearth of studies on reinforcing granite residual soils with fibers in alkaline solutions. In addition, the aforementioned researchers have only investigated the static load compressive strength of the treated granite residual soil, but little research has been conducted on the dynamic impact load performance of the reinforced soil and much less on its micromechanical characterization. Therefore, in this study, a comparison is made between glass fiber and basalt fiber in terms of GRS reinforcement in alkaline solution and the impact resistance of reinforced GRS under both static load and dynamic load, and the reinforcement mechanism of different fibers is examined from a microscopic perspective using SEM and XRD techniques as well.

2. Test Method

2.1. Materials

2.1.1. Granite Residual Soil. Granite residual soil has a distinctive structure and considerable strength in its dry state, but its strength drops rapidly after soaking in water or shaking (even if exposed to air for an extended period of time), causing engineering or geological disasters frequently. Consequently, it is considered "regional soil" or "unique soil." This experiment utilizes the granite residual soil excavated from the foundation pit of a Guangzhou subway station (Figure 1(a)). The soil is largely clayey and partially gravel clayey. It is primarily dark yellow in color. Its main soil mechanical properties are given in Table 1.

2.1.2. Sodium Hydroxide Analytical Reagent. Sodium hydroxide analytical reagent is a white (Figure 1(b)), uniform, granular solid that is water-soluble, has a density of 1.09 g/cm^3 and a molecular weight of 40, and forms a translucent aqueous solution upon dissolution in water.

2.1.3. Sodium Hydroxide Analytical Reagent. Sodium silicate analytical reagent is a white (Figure 1(c)), uniform, granular solid that is water-soluble, has a molecular weight of 284.22, contains around 64% of silicon dioxide and 22.5% of sodium oxide, and forms a translucent aqueous solution upon dissolution in water.

2.1.4. Basalt Fiber. Basalt fiber is an inorganic nonmetallic fiber material that is primarily manufactured from basalt ore that has been melted at a high temperature and then cast into a particular mold. It possesses outstanding characteristics such as high resilience strength, high modulus, resistance to high and low temperatures, and corrosion resistance. Its average length is 6 mm, and its diameter is 20 microns. The specific parameters of basalt fiber are shown in Table 2.

2.1.5. Glass Fiber. The glass fiber employed as the reinforcer in this experiment is an inorganic nonmetallic material with excellent performance, having an average length of 6 mm and a diameter of 10 microns, as shown in Figure 2. Nonpolluting and eco-friendly, it possesses excellent insulation, high heat resistance, superior corrosion resistance,

(a) (b) (c)

Figure 1: Material diagram: (a) granite residual soil, (b) sodium hydroxide, and (c) sodium metasilicate.

Table 1: Properties of granite residual soil samples.

Specific gravity (ds)	Water content ω (%)	Density (g/cm^3)	Liquid limit ω_1	Plastic limit (ωp)
2.67	13	16.5	48.3	27

Table 2: Fiber parameters.

Fiber type	Density (g/cm^3)	Linear density (dtex)	Elastic modulus (Mpa)	Tensile strength (Mpa)	Melting point (°C)	Elongation (%)
Basalt fiber	2.65	6.21	4500	330	958	30.0
Glass fiber	0.91	8.21	4286	346	169	36.4

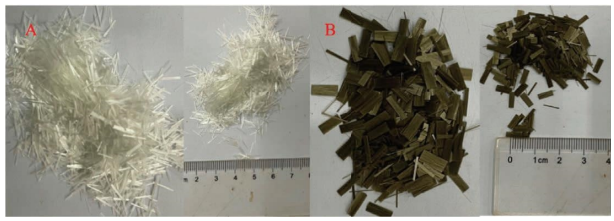

Figure 2: Material diagram: (a) glass fiber and (b) basalt fiber.

and high mechanical strength. The specific parameters of basalt fiber are given in Table 2.

2.2. Sample Preparation and Curing. In accordance with the Chinese Standard GB/T 50123-2019 (a standard for the geotechnical testing method), the samples were baked for 7 h at approximately 105°C and then crushed and sieved at 1.18 mm after cooling to room temperature. The 13% optimal water content used in this experiment was obtained in Yuan Bingxiang's previous research.

Different fibers and alkali solutions were added to the soil in varying amounts. The mixture was then well mixed, compacted into a cylinder with a diameter of 100 mm and a height of 50 mm using a geo-compaction equipment (Figure 3) in layers, and air-dried for 14 days in a well-ventilated indoor environment. The total weight of a sample is 1600 g.

2.3. Sample Numbering for the Unconfined Compressive Strength Test and the Drop-Weight Test. The optimal reinforcement ratio of the alkaline solution was determined by means of the unconfined compressive strength test as depicted in Table 3. For reinforcement, several molar ratios were used to prepare the alkaline solution. "0.5 mol" denotes an alkaline solution with a SiO_2/Na_2O ratio of 0.5 mol.

Table 4 illustrates the results of the drop-weight impact load test. The ideal content and length of glass fiber for reinforcement are 3% and 6 mm, whereas those of basalt fiber are 4% and 6 mm (chen et al). The optimal ratio of the alkaline solution determined by the static load test was 0.5 mol; hence, 0.5 mol alkaline solution was selected as the principal item for examination in the drop-weight test, alongside 0.7 mol and 0.4 mol alkaline solutions for comparison. In order to investigate the reinforcement effect of different fibers on granite residual soil in alkaline solution, glass fiber and basalt fiber were, respectively, incorporated into the soil based on the given ratios of alkaline solution. There are three examples for each condition. To label the samples, the drop-weight test was designated as "LC," the 0.7 mol alkaline solution ratio "0.7," and the addition of glass fiber and basalt fibers, "G" and "B", respectively. "GRS" refers to the pure soil sample. For instance, "LC-0.5-G" represents a sample containing glass fiber and an alkaline solution with a 0.5 mol ratio.

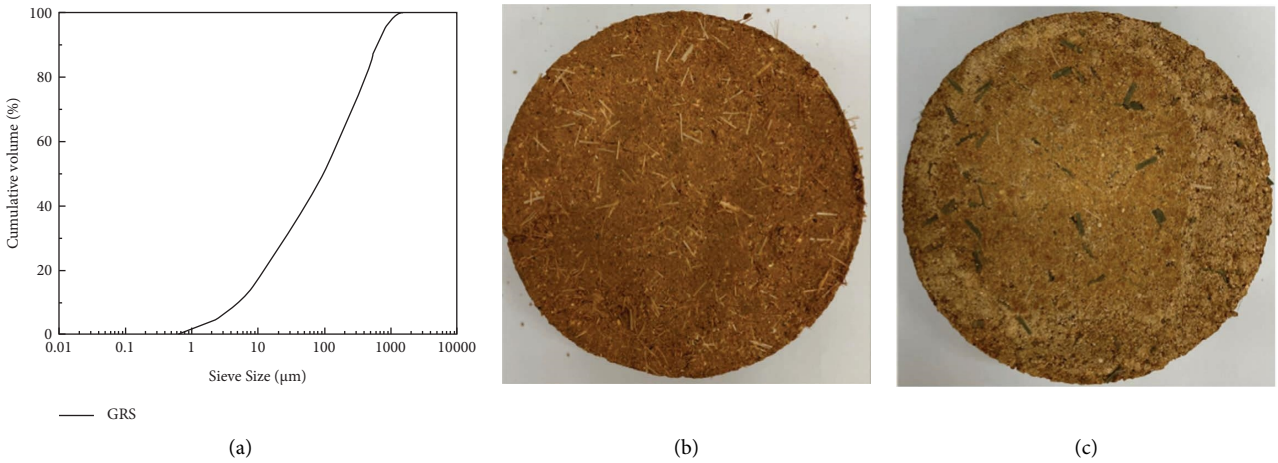

Figure 3: (a) GRS size, (b) glass fiber sample, and (c) basalt fiber sample.

Table 3: The unconfined compressive strength test plan.

	Group	Specimen number	Na_2SiO_3 (g)	NaOH (g)
Unconfined compressive strength tests	A	GRS	0	0
	B	2 mol	40	5.76
	C	1 mol	40	22.24
	D	0.7 mol	40	38.72
	E	0.5 mol	40	55.20
	F	0.4 mol	40	71.68

2.4. Method

2.4.1. Unconfined Compressive Strength Test. The uniaxial compressive strength of the sample was measured by a 4 W uniaxial compressive test instrument (see Figure 4). In accordance with GB/T 50123-2019 Standard for geotechnical testing methods, the sample was positioned in the exact center of the pressure plate of the press to rule out the possibility of eccentric loading at the loading rate of 0.5 MPa/s. The loading axial force at failure was recorded. The uniaxial compressive strength of each sample was calculated using the following formula:

$$R = \frac{P}{A}, \tag{1}$$

R is the ultimate compressive strength of the sample, P is the maximum load when the sample failed, and A is the cross-sectional area of the sample.

Based on the principle that the limit load should not exceed 15%, the average strength of three samples under the same ratio was calculated. To determine the optimal concentration of the alkaline solution, the unconfined compressive strength test was utilized to analyze the compressive strength of the samples at various ratios.

2.4.2. Drop-Weight Impact Test. The drop-weight test was conducted on an Instron Ceast 9350 floor-standingdrop-weight impact tester with a falling weight of 3.06 kg and a loading weight of 36.67 kg. The falling velocity was 4.5 m/s, and the corresponding instantaneous impact energy was 403.13 J. The pressure sensor on the surface of the falling weight recorded the impact load of samples, and the deformation was calculated by a computer (see Figure 5).

3. Results

3.1. Unconfined Compressive Strength Test. The GRS samples in Group A had a maximum compressive strength of 851.80 kPa. The maximum compressive strength of Group B, C, D, and E was 761.40 kPa, 1156.10 kPa, 4112.55 kPa, 4402.85 kPa, and 1750.70 kPa, respectively, when the alkali content was 2 mol, 1 mol, 0.7 mol, 0.5 mol, and 0.4 mol. Figure 6 depicts the maximum stress and error analysis of samples with varying SiO_2/Na_2O ratios in each group. Therefore, the effect of reinforcement on soil varies with the SiO_2/Na_2O ratio and is notable at the optimal ratio. Moreover, as seen in Figure 6, the addition of NaOH decreased the ratio of SiO_2/Na_2O by increasing the amount of Na_2O in the solution. A marked increase was witnessed when the ratio of SiO_2/Na_2O was reduced from 2 mol to 0.5 mol. The strength of samples comprising 0.7 mol and 0.5 mol SiO_2/Na_2O was almost 280% greater than that of samples comprising 2 mol and 1 mol SiO_2/Na_2O. However, the strength reduced to 1750.70 kPa when the ratio of SiO_2/Na_2O was increased to 0.4 mol, demonstrating that the ratio of SiO_2/Na_2O greatly enhances the strength and reinforcement effect only within a defined range and is not directly proportionate to the increase in strength. Based on the results of the unconfined compressive strength test, it was concluded that the ideal ratio of SiO_2/Na_2O for the

Table 4: The drop-weight test plan.

	Group	Specimen number	Na_2SiO_3 (g)	NaOH (g)	Glass fiber	Basalt fiber
Drop-weight test	H	LC-0.7-G	40	38.72	3	0
	I	LC-0.5-G	40	55.20	3	0
	J	LC-0.4-G	40	71.68	3	0
	K	LC-0.7-B	40	38.72	0	4
	L	LC-0.5-B	40	55.20	0	4
	M	LC-0.4-B	40	71.68	0	4
	N	GRS	0	0	0	0

alkaline solution's reinforcing effect on granite residual soil was 0.5 mol SiO_2/Na_2O.

3.2. Drop-Weight Test. Figures 7(a)–7(c) illustrate the ultimate bearing capacity of the specimens enhanced by different fibers under the differing ratios of alkali solution and impacted at an initial velocity of 4.5 m/s and an initial energy of 403.13 J, as well as the unreinforced GRS sample. As demonstrated in Figure 7(a), GRS has a bearing capacity of just 13.5 kN and deforms by 14 mm when subjected to an impact.

As shown in Figure 7(b), the addition of three molar ratios of alkaline solutions considerably improved the ultimate bearing capacity of glass fiber samples (LC-0.7-G, LC-0.5-G, and LC-0.4-G) in comparison to the GRS sample (40.6 kN, 120.0 kN, and 50.0 kN), with LC-0.5-G exhibiting the best reinforcement effect. This implies that the samples reinforced with an alkaline solution of 0.5 mol, SiO_2/Na_2O, and glass fiber were the strongest. In comparison to the deformation of the GRS sample (14.5 mm), the deformation of the samples containing glass fiber and alkali solution in three different ratios was reduced by 16.6% to 12.1 mm. The LC-0.5-G showed the least amount of distortion among them. It is possible to conclude that the addition of glass fiber and an alkaline solution containing 0.5 mol of SiO_2/Na_2O enhanced the reinforcing capacity of GRS in terms of both strength and deformation.

Figure 7(c) displays the impact resistance performance of GRS reinforced with basalt fiber in diverse alkaline solution ratios. The ultimate bearing capacities of the LC-0.7-B, LC-0.5-B, and LC-0.4-B increased by 211%, 507%, and 189%, respectively, compared to the GRS sample, to 42 kN, 82 kN, and 39 kN. LC-0.7-B exhibited the strongest reinforcing effect and the greatest ultimate bearing capacity. Despite the fact that LC-0.5-B has a greater bearing capacity, it appears that its deformation has not improved, as it has remained at around 14 mm. Similar conditions exist in the other two groups (LC-0.7-G and LC-0.4-G). Glass fiber has more advantages in enhancing the deformation of the samples than basalt fibers. In terms of bearing capacity, the optimal ratio of Si_2O/NaO_2 is 0.5 mol for the two kinds of fibers. This suggests that the optimal alkaline solution ratio for reinforcement is 0.5 mol Si_2O/NaO_2, which is consistent with the conclusion of the unconfined compressive strength test. The best reinforcement effect of the two fibers occurs in a 0.5 mol Si_2O/NaO_2 alkaline solution, but the reinforcement effect of glass fiber is superior, as evidenced by

Figure 4: uniaxial compression test instrument.

the fact that the ultimate bearing capacity and deformation of LC-0.5-G are 120 kN and 12.1 mm, or 46.3% and 13.6% higher than those of basalt fiber. In the optimal alkaline solution, it can be observed that glass fiber has a stronger reinforcing capacity than basalt fiber.

Figures 7(b) and 7(c) further demonstrate the relationship between impact force and deformation when a falling weight impacted the sample reinforced with various fibers and alkaline solutions. In each impact test, the compression deformation increased as the impact force increased. However, the decrease in impact force also resulted in a reduction in compression deformation. After an impact load was applied to the sample, pore compression and soil particle rearrangement would occur. These force-displacement curves can be divided into four distinct phases: the rearrangement phase, the increasing phase, the peak phase, and the weakening phase. Even though different types of fibers and an alkaline solution were employed to reinforce GRS, their impact forces and deformation curves are comparable as shown in Figures 7(b) and 7(c). In the deformation range of 0 to 2 mm, it is evident that the impact load of glass fiber samples (except for LC-0.5-G) rose sharply, reached the initial peak load, and then declined. Following its initial descent, the load ascended once more to an ultimate peak load of approximately 9 mm of deformation before the load dropped to 0 and remaining there ever since. The final deformation of the glass fiber sample was 12.1 mm. Within the 0–2 mm deformation range, the curves for basalt fiber samples went straight up, reached the

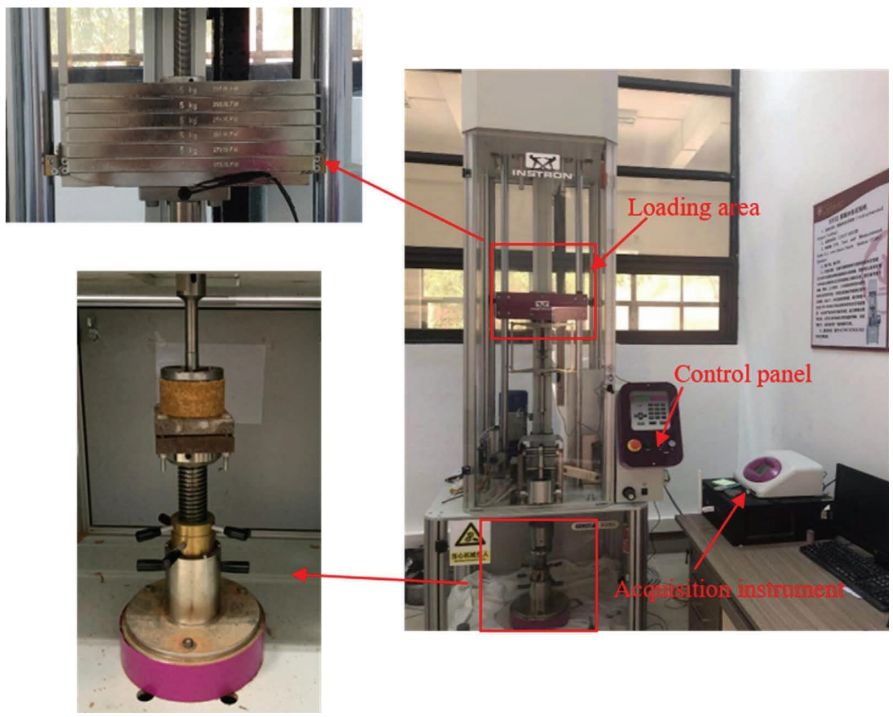

Figure 5: drop-weight tester.

first peak load, and then declined. After reaching the first lower point, the load climbed again, reached the ultimate peak load, and then dropped to 0 as the deformation increased to 14 mm.

As a result of the occurrence of instantaneous elastic deformation, the initial growth of the curves was approximately linear. At this point, the external force disturbed the soil granules, causing them to move and tumble, after which the granules rearranged and aggregated. As the pores narrowed and the effective stress between particles increased, the impact load increased linearly. After the elastic deformation reached its maximum, the impact force began to diminish because cracks in the samples exacerbated the compression deformation, resulting in a gradual decrease in the impact load. The impact load rebounded at approximately 2 mm of deformation and then increased to its maximum peak. This is because the soil was compacted, and its deformation modulus increased after it cracked to a certain extent. The mixture of glass fibers and soil absorbed the impact of the falling weight, allowing the sample to be further compressed without being destroyed.

However, the reinforcement effects of LC-0.5-G were different from LC-0.7-G and LC-0.4-G in the glass-fiber reinforced group, with LC-0.5-G being approximately 4 mm deformed at the rearrangement stage and LC-0.7-G and LC-0.4-G being approximately 1.5 mm deformed at that stage. This difference in reinforcement effects suggests that LC-0.5-G was more densely compacted, so there is less chance that the soil will move, roll, or tumble when resisting an external stress. As a result, the Si_2O/NaO_2 ratio of 0.5 mol produces the strongest reinforcement effect of glass fiber since this is

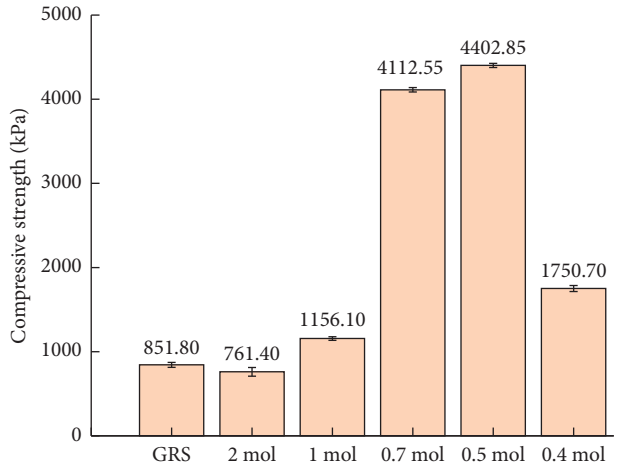

Figure 6: Compressive strength.

the ratio at which alkaline solution and glass fiber can work together most efficiently. It is determined that glass fiber and a 0.5 mol Si_2O/NaO_2 alkaline solution exhibit the maximum GRS reinforcing effect.

The optimal reinforcement effects of the two types of fibers added in the increase phase and the peak phase differ noticeably from one another. In samples of basalt fiber, the impact force gradually rose, and its deformation also dramatically increased to 14 mm with a maximum ultimate bearing capacity of just 82 kN. The final deformation of the glass fiber group, however, was only 12.1 mm when its impact force reached the maximum, over 13.6% lower than the basalt fiber. This is due to the fact that kaolinite in GRS

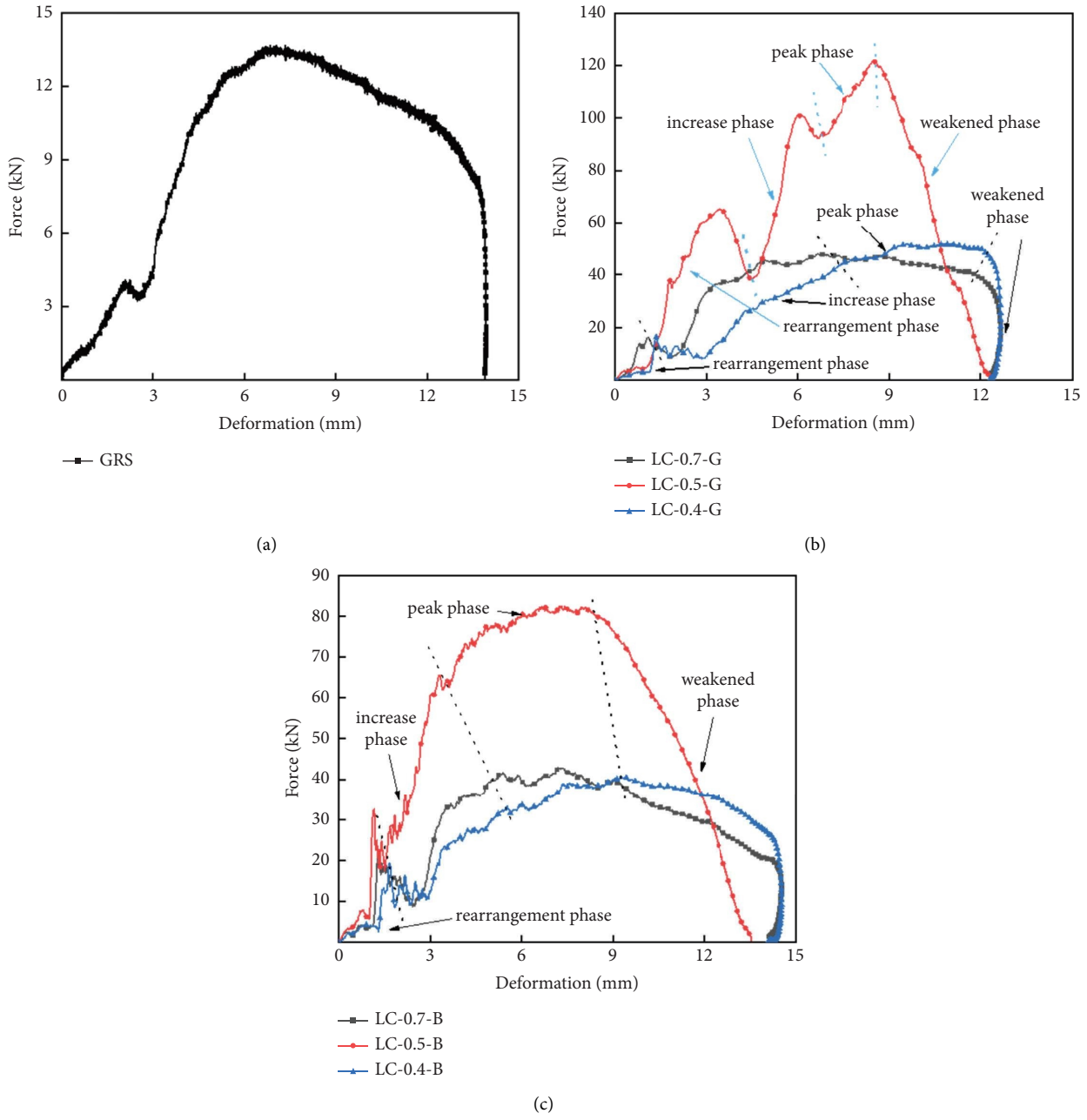

Figure 7: The diagram of impact force and compression deformation of the specimen.

was consumed and produced a gel substance under a 0.5 mol SiO_2/NaO_2 alkaline solution. Smaller glass fibers and the gel substance tightly and more firmly bind the soil together. Compared to glass fiber, which is assumed to have a better reinforcement capacity, basalt fiber's reinforcement effect is weaker under the optimal alkaline solution environment.

3.3. Scanning Electron Microscope. The SME images of GRS (Figure 8) reveal that the soil in the GRS sample is composed of granular particles with weak interaction. Under a microscope, the shape of the particles is hexagonal flaky or incomplete hexagonal flaky. This may be explained by the large amount of kaolinite in GRS. Kaolinite is in a hexagonal shape itself, and its incomplete hexagonal shape could be attributed to the compression and destruction of the soil during excavation that changes morphology. It was found that GRS contains a large amount of kaolinite, which is consistent with the results of XRD analysis.

The sample failed because it could not bear the impact load due to the relatively weak connection between soil particles in the original state of GRS. In contrast, the SEM images of the glass fiber group and the basalt fiber group (Figure 9) demonstrated that the soil mass remained relatively intact after being subjected to an external load and that a gel substance bound the soil particles and glass fibers into a cohesive whole that collectively bears the external impact load. The inclusion of fibers into the soil assisted in

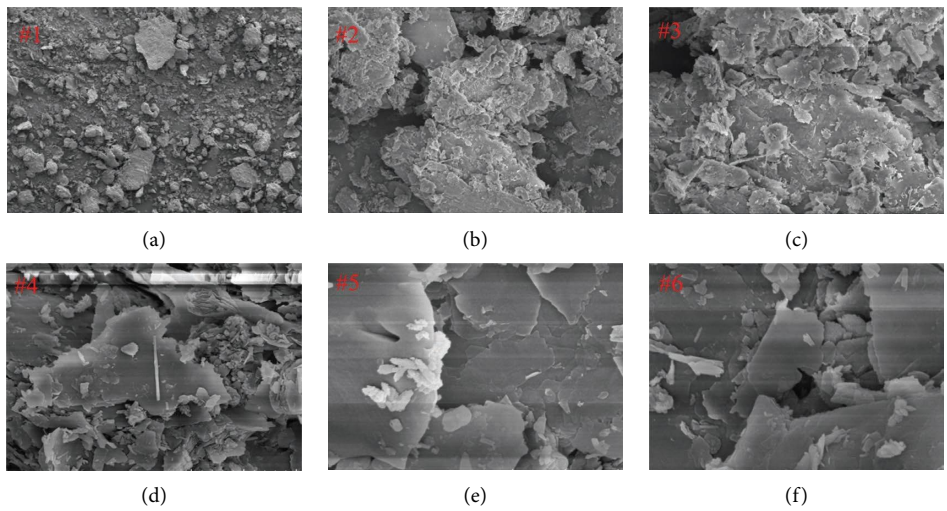

Figure 8: SEM images of material (GRS).

reinforcing the soil, thus enhancing the sample's structural integrity and, consequently, its ultimate bearing capacity.

In Figure 9, it is noticed that more glass fibers attached to the soil compared to the basalt fibers. The gel substance that formed after the addition of glass fiber to an alkaline solution may have bonded the soil particles and fibers closely and filled the pores, thereby increasing the compactness of the sample. In addition, the mixture of gel, soil particles, and fibers bears the load collectively, and the load can be transferred from soil to fiber and gel. Due to the high tensile strength of fibers and gel, the sample exhibits outstanding deformation under impact load, which explains why LC-0.5-G exhibits greater deformation than other samples. Due to the close combination of gel, fiber, and soil particles, a greater impact force is required to rearrange its particles when subjected to stress, which translates to a higher bearing capacity in mechanics. In comparison, basalt fiber samples contained less gel substance and fewer soil particles adhering to the surface of the fibers, resulting in a weaker connection between fiber and soil and a lower resistance to impact loads than glass fiber samples. The SME analysis provided additional understanding into the different reinforcing effects of glass fiber and basalt fibers on GRS in alkaline solution and revealed the reinforcement mechanism of the two fibers on GRS from a microscopic perspective.

3.4. XRF and XRD. XRF (Figure 10) results suggest that GRS (Figure 10(b)) contains a significant amount of silicon and aluminum, similar to the composition of MK (Figure 10(a)). In conjunction with the SEM and XRD analyses (Figures 11(a) and 11(b)), it is evident that GRS contains a significant amount of kaolinite, which was consumed and formed a gel with adhesion upon alkaline solution reinforcement.

Based on the results of the preceding analysis, the reinforcing effect of glass fiber in an alkaline solution is superior to that of basalt fiber; thus, only the group with the best reinforcement effect (LC-0.5-G) is chosen for XRD analysis. GRS is mostly composed of the minerals kaolinite, quartz, and a little amount of illite and low sodium potassium feldspar, according to the standard PDF of XRD, with kaolinite accounting for more than 50% of the total. Compared to the GRS sample, the kaolinite in sample LC-0.5-G exhibits multiple reflections, the strongest of which occurs at 12.3°. Although their reflection angle remained unchanged, their reflection intensity reduced dramatically, indicating a decrease in the crystallinity and content of kaolinite. A plausible explanation is that the alkaline solution consumes kaolinite particles, lowering the crystallinity of the kaolinite as a result. Microscopically, soil particles become more stable and solid, enhancing the sample's overall strength.

The quartz phase in LC-0.5-G was essentially similar to GRS and was integral, but the reflection intensity was greatly reduced, suggesting that the crystallinity and content of quartz have decreased. The most likely reason is that when kaolinite particles are mixed with alkali solution (0.5 mol SiO_2/Na_2O), the new substances formed had effect on the quartz reflection peak. Consequently, the intensity of the peak was diminished in XRD, but quartz is fundamentally stable, hence no significant change was seen.

At the reflection of 27.8°, a considerable increase in potassium feldspar content was observed, showing that the addition of alkaline solution promoted the formation of potassium feldspar in the sample, as evidenced by the sharp and noticeable potassium feldspar reflection peaks. Potassium feldspar belongs to the monoclinic crystal system, whose main components are alumina, silicon dioxide, and potassium oxide, and is distinguished by its high stability, high strength, and outstanding compressive performance. The majority of the substances in LC-0.5-G, quartz, and potassium feldspar are stable. The gel substance and geopolymer formed in LC-0.5-G had high viscosity and strength; they filled the pores of the particles and adhered them more firmly, thus significantly increasing the effective stress and enhancing the soil's strength.

From a microscopic perspective, the addition of a 0.5 mol, SiO_2/Na_2O alkaline solution and glass fiber

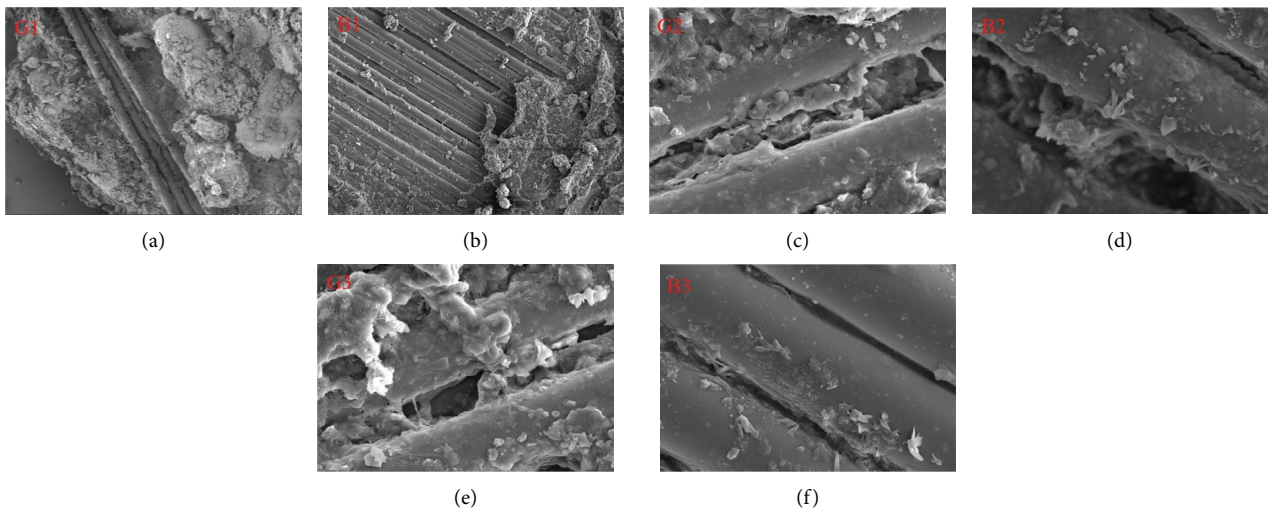

Figure 9: SEM of reinforcement soil of glass fiber (a), (c), and (e) and basalt fiber (b), (d), and (f).

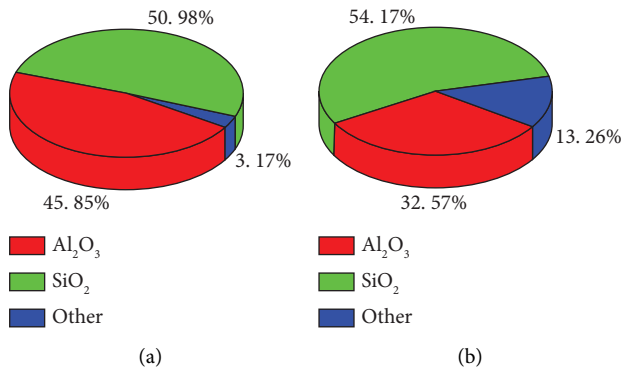

Figure 10: XRF patterns of MK (a) and GRS (b).

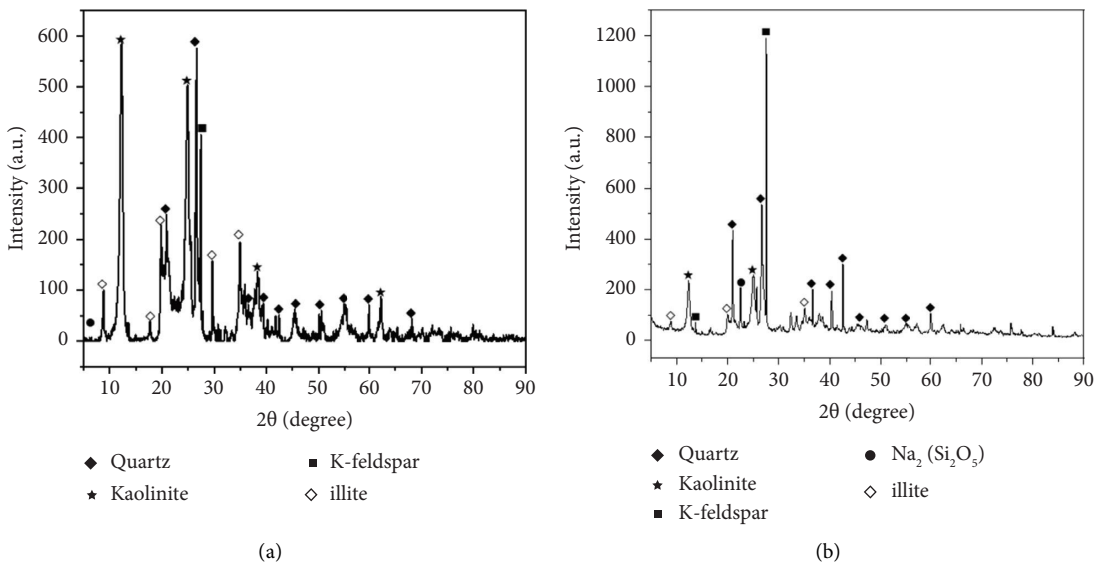

Figure 11: XRD patterns of GRS (a) and LC-0.5-G (b).2

produced more substances with greater strength and stability. Under the viscous envelopment of the geopolymer, the soil mixture formed a whole with enhanced compressive strength and stability.

The reasons for the distinct reinforcement effects of two different fibers on GRS in alkaline solution have been described from a macroperspective to microperspective. It was concluded that the reinforcing effect of glass fiber with GRS in an alkaline solution is superior to basalt fiber.

4. Conclusion

This article investigates the reinforcement effects of two different fibers on GRS in an alkaline solution, the influence of the SiO_2/Na_2O ratio in an alkaline solution on reinforcement performance, and the influence of glass fiber and basalt fiber on the mechanical properties of GRS in an alkaline solution and its microscopic mechanism using an unconfined compressive strength test and a drop-weight impact load test.

(1) The static load test showed that the samples' ultimate bearing capacity reached their highest value of 4402.85 kpa under a 0.5 mol SiO_2/Na_2O alkaline solution compared to samples of pure soil. Therefore, 0.5 mol of SiO_2/Na_2O is the ideal concentration for an alkaline solution.

(2) The drop-weight impact test demonstrates that the ultimate impact bearing capability of GRS is greatly enhanced after basalt fiber and glass fiber reinforcement in the optimal alkaline solution. Among them, the reinforcement effect of glass fiber is the most successful, as evidenced by the sample's deformation decreasing by 13.6% to 12.1 mm and its ultimate strength increasing by 789% to 120 kN.

(3) The significant increase in strength, as shown by SEM and XRD, is a result of the relatively high tensile strength of the glass fiber and the formation of a gel near the glass fiber in the alkaline solution, which binds the soil particles more closely and forms a whole that collectively bears the external load, thereby increasing the sample's strength. The smaller diameter of the glass fiber facilitates a better connection between the fiber and the soil particle. Basalt fiber, on the other hand, serves only as a connecting component during reinforcement because it does not produce an additional gel that binds the fibers together. Therefore, the reinforcement effect of basalt fiber with GRS in an alkaline solution is inferior to that of glass fiber.

Data Availability

The data supporting the findings of the current study are available from the corresponding author upon request.

Conflicts of Interest

The authors declare that there are no conflicts of interest.

Acknowledgments

The authors would gratefully like to acknowledge the support provided by the National Natural Science Foundation of China (51978177 and 41902288) and the Guangzhou Basic and Applied Basic Research Project (202201010391).

References

[1] S. Nanda and F. Berruti, "Municipal solid waste management and landfilling technologies: a review," *Environmental Chemistry Letters*, vol. 19, no. 2, pp. 1433–1456, 2020.

[2] L. C. Dang, H. Khabbaz, and B. J. Ni, "Improving engineering characteristics of expansive soils using industry waste as a sustainable application for reuse of bagasse ash," *Transportation Geotechnics*, vol. 31, Article ID 100637, 2021.

[3] R. Chen, S. S. C. Congress, G. Cai, W. Duan, and S. Liu, "Sustainable utilization of biomass waste-rice husk ash as a new solidified material of soil in geotechnical engineering: a review," *Construction and Building Materials*, vol. 292, Article ID 123219, 2021.

[4] Z. Nalbantoğlu, "Effectiveness of Class C fly ash as an expansive soil stabilizer," *Construction and Building Materials*, vol. 18, no. 6, pp. 377–381, 2004.

[5] P. Ghadir and N. Ranjbar, "Clayey soil stabilization using geopolymer and Portland cement," *Construction and Building Materials*, vol. 188, pp. 361–371, 2018.

[6] J. Xiao, J. Shen, M. Bai, Q. Gao, and Y. Wu, "Reuse of construction spoil in China: c," *Journal of Cleaner Production*, vol. 290, Article ID 125742, 2021.

[7] Q. Dong, G. Wang, X. Chen, J. Tan, and X. Gu, "Recycling of steel slag aggregate in portland cement concrete: an overview," *Journal of Cleaner Production*, vol. 282, Article ID 124447, 2021.

[8] E. S. Santos Nascimento, P. C. D. Souza, H. A. D. Oliveira, C. M. Melo Junior, V. G. D. Oliveira Almeida, and F. M. C. D. Melo, "Soil-cement brick with granite cutting residue reuse," *Journal of Cleaner Production*, vol. 321, Article ID 129002, 2021.

[9] C. S. Vieira, P. M. Pereira, and M. D. L. Lopes, "Recycled Construction and Demolition Wastes as filling material for geosynthetic reinforced structures. Interface properties," *Journal of Cleaner Production*, vol. 124, pp. 299–311, 2016.

[10] R. Muduli and B. B. Mukharjee, "Effect of incorporation of metakaolin and recycled coarse aggregate on properties of concrete," *Journal of Cleaner Production*, vol. 209, pp. 398–414, 2019.

[11] X. Liu, X. Zhang, L. Kong, G. Wang, and J. Lu, "Disintegration of granite residual soils with varying degrees of weathering," *Engineering Geology*, vol. 305, Article ID 106723, 2022.

[12] X. Liu, X. Zhang, L. Kong, G. Wang, and H. Liu, "Formation mechanism of collapsing gully in southern China and the relationship with granite residual soil: a geotechnical perspective," *Catena*, vol. 210, Article ID 105890, 2022.

[13] J. Xia, C. Cai, Y. Wei, and X. Wu, "Granite residual soil properties in collapsing gullies of south China: spatial variations and effects on collapsing gully erosion," *Catena*, vol. 174, pp. 469–477, 2019.

[14] B. Zhang, H. Guo, L. Deng, W. Fan, T. Yu, and Q. Wang, "Undehydrated kaolinite as materials for the preparation of geopolymer through phosphoric acid-activation," *Applied Clay Science*, vol. 199, Article ID 105887, 2020.

[15] Y. Wei, X. Wu, J. Xia et al., "The effect of water content on the shear strength characteristics of granitic soils in South China," *Soil and Tillage Research*, vol. 187, pp. 50–59, 2019.

[16] Y. Yao, J. Ni, and J. Li, "Stress-dependent water retention of granite residual soil and its implications for ground settlement," *Computers and Geotechnics*, vol. 129, Article ID 103835, 2021.

[17] B. Yuan, Z. Li, Y. Chen et al., "Mechanical and microstructural properties of recycling granite residual soil reinforced with glass fiber and liquid-modified polyvinyl alcohol polymer," *Chemosphere*, vol. 286, no. P1, Article ID 131652, 2022.

[18] B. Yuan, W. Chen, J. Zhao et al., "Addition of alkaline solutions and fibers for the reinforcement of kaolinite-containing granite residual soil," *Applied Clay Science*, vol. 228, Article ID 106644, 2022.

[19] B. Yuan, W. Chen, Z. Li et al., "Sustainability of the polymer SH reinforced recycled Granite Residual Soil: properties, physicochemical mechanism and applications," *Journal of Soils and Sediments*, vol. 23, no. 1, pp. 246–262, 2023.

[20] B. Yuan, M. Chen, W. Chen, Q. Luo, and H. Li, "Effect of pile-soil relative stiffness on deformation characteristics of the laterally loaded pile," *Advances in Materials Science and Engineering*, vol. 2022, Article ID 4913887, 13 pages, 2022.

[21] B. Yuan, M. Sun, Y. Wang, L. Zhai, Q. Luo, and X. Zhang, "Full 3D displacement measuring system for 3D displacement field of soil around a laterally loaded pile in transparent soil," *International Journal of Geomechanics*, vol. 19, no. 5, Article ID 04019028, 2019.

[22] B. Yuan, Z. Li, W. Chen et al., "Influence of groundwater depth on pile–soil mechanical properties and fractal characteristics under cyclic loading," *Fractal and Fractional*, vol. 6, no. 4, p. 198, 2022.

[23] Y. Wu, J. Cui, J. Huang, W. Zhang, N. Yoshimoto, and L. Wen, "Correlation of critical state strength properties with particle shape and surface fractal dimension of clinker ash," *International Journal of Geomechanics*, vol. 21, no. 6, Article ID 04021071, 2021.

[24] X. Que, Z. Zhu, Z. Niu, and W. Lu, "Estimating the strength and deformation of columnar jointed rock mass based on physical model test," *Bulletin of Engineering Geology and the Environment*, vol. 80, no. 2, pp. 1557–1570, 2021.

[25] L. Wang, Z. Yu, B. Liu, F. Zhao, S. Tang, and M. Jin, "Effects of fly ash dosage on shrinkage, crack resistance and fractal characteristics of face slab concrete," *Fractal Fract*, vol. 6, p. 335, 2022.

[26] L. Wang, S. Zhou, Y. Shi et al., "The influence of fly ash dosages on the permeability, pore structure and fractal features of face slab concrete," *Fractal Fract*, vol. 6, no. 9, p. 476, 2022.

[27] L. Wang, G. Li, X. Li et al., "Influence of reactivity and dosage of MgO expansive agent on shrinkage and crack resistance of face slab concrete," *Cement and Concrete Composites*, vol. 126, Article ID 104333, 2022.

[28] L. Wang, T. S. He, Y. X. Zhou et al., "The influence of fiber type and length on the cracking resistance, durability and pore structure of face slab concrete," *Construction and Building Materials*, vol. 282, Article ID 122706, 2021.

[29] B. B. Yang and Y. Liu, "Application of fractals to evaluate fractures of rock due to mining," *Fractal and Fractional*, vol. 6, no. 2, p. 96, 2022.

[30] B. B. Yang, J. Liu, X. Zhao, and S. Zheng, "Evaporation and cracked soda soil improved by fly ash from recycled materials," *Land Degradation & Development*, vol. 32, no. 9, pp. 2823–2832, 2021.

[31] B. B. Yang, S. Du, X. Zhao, D. Tang, and C. Yang, "Decision making of curriculum attainment degree for engineering geology based on fuzzy set theory," *Advances in Civil Engineering*, vol. 20216 pages, Article ID 1743778, 2021.

[32] F. Liu, G. Chen, L. Li, and Y. Guo, "Study of impact performance of rubber reinforced concrete," *Construction and Building Materials*, vol. 36, no. 11, pp. 604–616, 2012.

[33] Z. Lu, W. H. Zhou, and Z. Y. Yin, "Effect of viscosity on slurry infiltration in granular media," *International Journal of Geomechanics*, vol. 22, no. 9, Article ID 04022138, 2022.

[34] Z. Lu, W. H. Zhou, Z. Y. Yin, and J. Yang, "Numerical modeling of viscous slurry infiltration in sand," *Computers and Geotechnics*, vol. 146, Article ID 104745, 2022.

[35] H. Guo, B. Zhang, L. Deng, P. Yuan, M. Li, and Q. Wang, "Preparation of high-performance silico-aluminophosphate geopolymers using fly ash and metakaolin as raw materials," *Applied Clay Science*, vol. 204, Article ID 106019, 2021.

[36] B. X. Yuan, W. J. Chen, J. Zhao, F. Yang, Q. Luo, and T. Chen, "The effect of organic and inorganic modifiers on the physical properties of granite residual soil," *Advances in Materials Science and Engineering*, vol. 2022, Article ID 9542258, 13 pages, 2022.

[37] Y. S. Kim, T. Q. Tran, G. O. Kang, and T. M. Do, "Stabilization of a residual granitic soil using various new green binders," *Construction and Building Materials*, vol. 223, pp. 724–735, 2019.

[38] S. Hov, P. Paniagua, C. Sætre et al., "Lime-cement stabilisation of Trondheim clays and its impact on carbon dioxide emissions," *Soils and Foundations*, vol. 62, no. 3, Article ID 101162, 2022.

[39] S. Nie, J. Zhou, F. Yang et al., "Analysis of theoretical carbon dioxide emissions from cement production: m," *Journal of Cleaner Production*, vol. 334, Article ID 130270, 2022.

[40] B. Zhang, H. Guo, P. Yuan et al., "Geopolymerization of halloysite via alkali-activation: d," *Applied Clay Science*, vol. 185, Article ID 105375, 2020.

[41] B. Zhang, Y. Feng, J. Xie et al., "Effects of fibres on ultra-lightweight high strength concrete: dynamic behaviour and microstructures," *Cement and Concrete Composites*, vol. 128, Article ID 104417, 2022.

[42] M. Ohno and V. C. Li, "A feasibility study of strain hardening fiber reinforced fly ash-based geopolymer composites," *Construction and Building Materials*, vol. 57, pp. 163–168, 2014.

[43] Z. Chen, H. Zhou, F. Ye, B. Liu, and W. Fu, "The characteristics, induced factors, and formation mechanism of the 2018 Baige landslide in Jinsha River, Southwest China," *Catena*, vol. 203, Article ID 105337, 2021.

[44] Z. Chen, H. Zhou, F. Ye, B. Liu, W. Fu, and M. Moscatelli, "Landslide susceptibility mapping along the anninghe fault zone in China using SVM and ACO-PSO-SVM models," *Lithosphere*, vol. 2022, no. 1, Article ID 5216125, 2022.

[45] A. Saludung, T. Azeyanagi, Y. Ogawa, and K. Kawai, "Alkali leaching and mechanical performance of epoxy resin-reinforced geopolymer composite," *Materials Letters*, vol. 304, Article ID 130663, 2021.

[46] S. Samal, "Interface failure and delamination resistance of fiber-reinforced geopolymer composite by simulation and experimental method," *Cement and Concrete Composites*, vol. 128, Article ID 104420, 2022.

[47] S. Narani, M. Abbaspour, S. M. Mir Mohammad Hosseini, E. Aflaki, and F. Moghadas Nejad, "Sustainable reuse of Waste Tire Textile Fibers (WTTFs) as reinforcement materials for expansive soils: with a special focus on landfill liners/covers,"

Journal of Cleaner Production, vol. 247, Article ID 119151, 2020.

[48] R. Mattone, "Sisal fibre reinforced soil with cement or cactus pulp in bahareque technique," *Cement and Concrete Composites*, vol. 27, no. 5, pp. 611–616, 2005.

[49] M. F. Ma'Ruf, "Shear strength of Apus bamboo root reinforced soil," *Ecological Engineering*, vol. 41, pp. 84–86, 2012.

[50] M. Mirzababaei, A. Arulrajah, A. Haque, S. Nimbalkar, and A. Mohajerani, "Effect of fiber reinforcement on shear strength and void ratio of soft clay," *Geosynthetics International*, vol. 25, no. 4, pp. 471–480, 2018.

[51] K. Meng, C. Cui, Z. Liang, H. Li, and H. Pei, "A new approach for longitudinal vibration of a large-diameter floating pipe pile in visco-elastic soil considering the three-dimensional wave effects," *Computers and Geotechnics*, vol. 128, Article ID 103840, 2020.

[52] C. Cui, K. Meng, Y. J. Wu, D. Chapman, and Z. M. Liang, "Dynamic response of pipe pile embedded in layered visco-elastic media with radial inhomogeneity under vertical excitation," *Geomechanics and Engineering*, vol. 16, no. 6, pp. 609–618, 2018.

[53] N. Jain, A. Verma, and V. K. Singh, "Dynamic mechanical analysis and creep-recovery behaviour of polyvinyl alcohol based cross-linked biocomposite reinforced with basalt fiber," *Materials Research Express*, vol. 6, no. 10, Article ID 105373, 2019.

[54] M. Karthick, M. Meikandan, S. Kaliappan et al., "Experimental investigation on mechanical properties of glass fiber hybridized natural fiber reinforced penta-layered hybrid polymer composite," *International Journal of Chemical Engineering*, vol. 2022, Article ID 1864446, 9 pages, 2022.

[55] A. Verma, A. Parashar, N. Jain, V. K. Singh, S. M. Rangappa, and S. Siengchin, "Surface modification techniques for the preparation of different novel biofibers for composites," *Biofibers and Biopolymers for Biocomposites: Synthesis, Characterization and Properties*, pp. 1–34, Springer International Publishing, Cham, Switzerland, 2020.